TiO_2 Anatase Nanoparticle Networks: Synthesis, Structure, and Electrochemical Performance

Pierre Kubiak, Thomas Fröschl, Nicola Hüsing, Ute Hörmann, Ute Kaiser, Renate Schiller, Clemens K. Weiss, Katharina Landfester, and Margret Wohlfahrt-Mehrens*

Nanocrystalline anatase TiO_2 materials with different specific surface areas and pore size distributions are prepared via sol–gel and miniemulsion routes in the presence of surfactants. The samples are characterized by X-ray diffraction, nitrogen sorption, transmission electron microscopy, and electrochemical measurements. The materials show a pure anatase phase with average crystallite size of about 10 nm. The nitrogen sorption analysis reveals specific surface areas ranging from 25 to 150 m^2 g^{-1}. It is demonstrated that the electrochemical performance of this material strongly depends on morphology. The mesoporous TiO_2 samples exhibit excellent high rate capabilities and good cycling stability.

1. Introduction

The goal of improving the efficiency of lithium-ion batteries, especially in terms of energy and power densities, lifetime, cost, and safety, has led to many efforts towards the development of novel electrode materials. A higher demand for efficient energy storage for the future market of hybrid electric vehicles (HEVs) and electric vehicles (EVs)[1] is among the principal reasons driving these efforts. There is an increasing interest in the development of alternative cathode and anode materials with enhanced kinetics and high rate capabilities. In this context, nanosized materials have attracted considerable attention due to their improved electrochemical properties when compared to bulk materials.[2] For nanosized materials small crystallite size leads to faster lithium insertion/extraction together with a large specific surface area that provides a greater electrode/electrolyte interface. Graphite-based anodes, which are currently used in Li-ion batteries, exhibit poor performance under operating conditions such as low temperatures and high charge/discharge rates. Furthermore, they also present high irreversible capacity in the first cycle due to the solid electrolyte interface (SEI) formation. Anode materials based on titanium oxides are promising candidates as alternative materials to carbonaceous anodes due to advantages in terms of cost, safety, and toxicity when compared to other anodic materials. Among the several polymorphs of TiO_2, brookite, TiO_2-B, anatase, and rutile are promising anode materials for Li-ion batteries.[3] Typically the Li^+ insertion/extraction reaction for TiO_2 polymorphs occurs in the potential range of 1.4–1.8 V vs. Li/Li^+, according to the following reaction:

$$x\,Li^+ + TiO_2 + x e^- = Li_x\,TiO_2 \qquad (1)$$

The maximum theoretical capacity is 335 mAh g^{-1}, which corresponds to $x = 1$ and to the complete reduction of Ti^{4+} to Ti^{3+}. This makes TiO_2 a highly competitive alternative to graphite anodes. The working potential of the cell depends on the TiO_2 polymorph used. TiO_2-B has an insertion potential of about 1.6 V vs. Li^+ associated with the Li^+ insertion into the structure. A composition of $Li_{0.91}TiO_2$ corresponding to 305 mAh g^{-1} has been reported for the first cycle with a reversible intercalation of approximately 0.7 mol Li^+ per

Dr. P. Kubiak, Dr. M. Wohlfahrt-Mehrens
ZSW-Zentrum für Sonnenenergie und Wasserstoff Forschung
Helmhotzstraße 8, 89081 Ulm, Germany
E-mail: Pierre.kubiak@zsw-bw.de
T. Fröschl, Prof. N. Hüsing
Institute of Inorganic Chemistry I
Ulm University
Albert Einstein Allee 11, 89081 Ulm, Germany
Dr. U. Hörmann, Prof. U. Kaiser
Electron Microscopy Group of Material Science
Ulm University
Albert Einstein Allee 11, 89081 Ulm, Germany
Dr. R. Schiller, Dr. C. K. Weiss, Prof. K. Landfester
Max-Planck-Institut für Polymerforschung
Ackermannweg 10, 55128 Mainz, Germany

DOI: 10.1002/smll.201001943

molecule of TiO_2.[4] Very few reports of electrochemical lithium insertion into TiO_2 brookite polymorph have been made.[5] Reddy et al. have reported a reversible capacity of 160–170 mAh g^{-1} at 1.7 V vs. Li/Li^+ for nanosized brookite samples. On the other hand, the rutile TiO_2 polymorph has been considered a poor Li insertion material for a long time. The reported capacity values for bulk rutile were in the range of ≈0.15 Li per molecule of TiO_2.[6] It is only recently that excellent capacities at high rates have been reported for TiO_2 rutile with nanosized dimensions.[7] Among the TiO_2 polymorphs, anatase is considered as the most promising candidate for use as an anode material for Li-ion batteries due to its fast Li^+ insertion/extraction reactions and high insertion capacity.[8] From the practical viewpoint, reversible insertion into anatase TiO_2 is about 0.6 Li (i.e., 200 mAh g^{-1}) at 1.78 V vs. Li^+/Li.[9] It has been demonstrated that the composition of Li_1TiO_2 can be obtained from anatase TiO_2 at high temperature[10] or with particle size inferior to 7 nm.[11]

The use of nanosized materials is not without complications, however. Reports of a decrease of the volumetric energy density due to a possible loss of connectivity between particles because of parasitic reactions with the electrolyte are well known.[12] Therefore, controlling the morphology appears to be crucial in determining the electrochemical performance of TiO_2 materials in Li-ion batteries. In this context, mesoporous materials have received particular attention since they are demonstrated to be an optimal morphology for increasing electrode stability and Li insertion capacity, especially at high charge/discharge rates.[13] Besides the control of morphology, different strategies have been studied to improve the electrochemical performance of mesoporous anatase: for example, mixing TiO_2 with Ag nanoparticles,[14] glassy-like phases,[15] RuO_2,[16] carbon,[17] spacers,[18] or using metal coatings.[19]

Herein, we demonstrate how to optimize the morphology of anatase TiO_2 nanosized materials to obtain excellent electrochemical lithium insertion/extraction performance. We utilize various synthetic conditions to obtain materials with different specific surface areas, particle sizes, and pore size distributions and investigate their electrochemical properties in order to correlate morphology and pore structure with their performance as anode materials.

2. Results and Discussion

2.1. Materials Characterization

To obtain different morphologies of TiO_2 anatase nanoparticles, different synthetic routes were utilized. TiO_2-a has been obtained via a sol–gel route using a glycol-modified titanium precursor (EGMT)[20] in the presence of a nonionic surfactant (Brij56).[21] A pure anatase phase with crystallite size of 9 nm (**Figure 1**) and a specific surface area of 110 m^2 g^{-1} was obtained. The nitrogen sorption results show isotherm curves characteristic of mesoporous materials with drop-shaped pores (**Table 1**) with a narrow pore size distribution of maximum 5 nm. TiO_2-b has been prepared via the sol–gel method with tetraisopropylorthotitanate as titanium precursor in the presence of octadecylamine.[22] The X-ray diffraction (XRD) patterns showed a pure anatase phase with average crystallite size of 10 nm (Figure 1) and low surface area (25 m^2 g^{-1}) due to nonporous morphology. TiO_2-c has been obtained via an inverse miniemulsion process.[23] The size of the crystallites is below 10 nm, as determined from transmission electron microscopy (TEM) images and the evaluation of the diffractograms with the Scherrer equation (Figure 1). The specific surface area was 150 m^2 g^{-1}, and the pore size distribution was broader than for TiO_2-a (7–15 nm) due to the particulate morphology of the material. XRD patterns of the prepared TiO_2 materials are shown in Figure 1. The physical properties of the studied samples are summarized in Table 1.

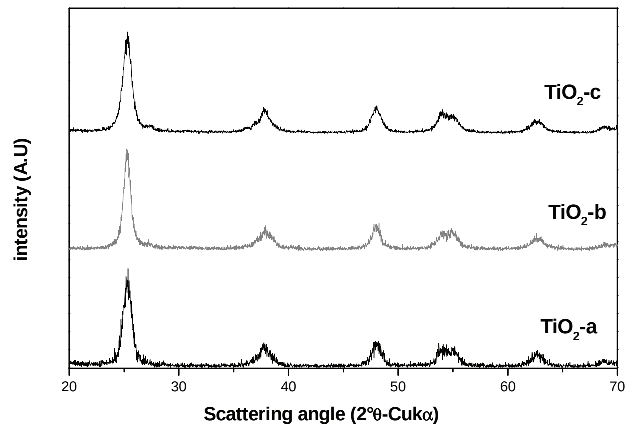

Figure 1. XRD patterns from samples TiO_2-a, TiO_2-b, and TiO_2-c.

The values of the average crystallite size determined by Scherrer's equation have been confirmed by TEM (**Figure 2**). Moreover, the images provide information about the connectivity between the nanocrystallites. Based on the TEM images, it can be clearly seen that TiO_2-a is mesoporous (indicated by arrows in Figure 2, middle).

2.2. Evaluation of Electrochemical Performance

The electrochemical evaluation of the three anatase materials with different porosities was carried out by both

Table 1. Structural properties of the different titanium oxides used in this study.

Sample	Polymorph	SSA (BET)[a)] [m^2 g^{-1}]	Pore diameter (BJH)[b)] [nm]	Crystallite size[c)] (XRD) [nm]	Particle size (TEM) [nm]
TiO_2-a	anatase	110	6,7	9	9
TiO_2-b	anatase	25	n.m.[d)]	10	10
TiO_2-c	anatase	150	7–15	10	12

[a)]SSA = specific surface area; BET = Brunauer–Emmett–Teller; [b)]BJH = Barrett–Joyner–Halenda; [c)]Determined by applying the Scherrer equation; [d)]n.m. = not measurable.

small

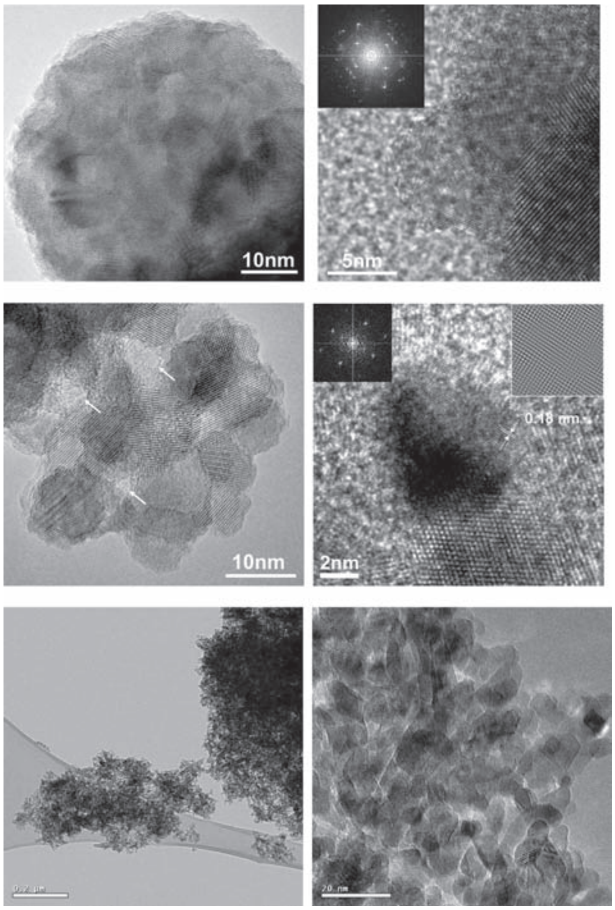

Figure 2. TEM images of TiO_2 aggregates. Top: TiO_2-b, nonporous spherically aggregated with densely packed anatase nanocrystallites. Inset: electron diffraction patterns. Middle: TiO_2-a, mesoporous loosely aggregated anatase. Arrows point to mesopores. Inset: electron diffraction patterns. Bottom: TiO_2-c, mesoporous loosely aggregated crystallites.

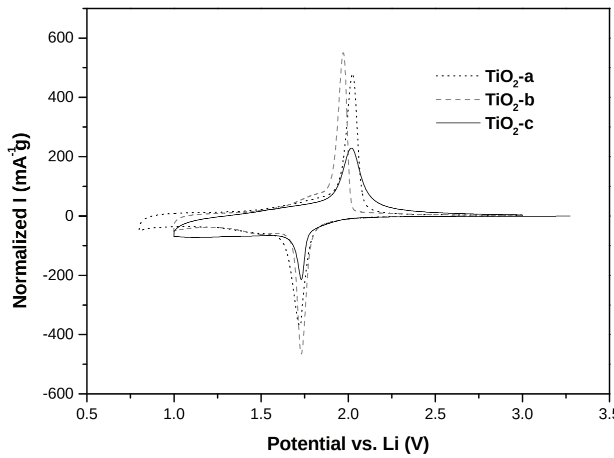

Figure 3. Comparison between cyclic voltammograms of TiO_2-a, TiO_2-b, and TiO_2-c at a scan rate $v = 0.1$ mV s^{-1}.

cyclic voltammetry and galvanostatic cycling. Cyclic voltammetry was carried out between 1 and 3 V at a scan rate of 0.1 mV s^{-1}. The comparison between the voltammograms is shown in **Figure 3**.

All three voltammograms presented two peaks at about 1.75 V (cathodic) and 2.0 V (anodic) corresponding to the faradaic insertion and extraction of lithium into anatase TiO_2.[24] Upon Li insertion, the anatase converts to a two-phase product, including the Li-poor Li $_{0.0x}$ TiO_2 (space group $I4_1/amd$) phase with tetragonal symmetry, and the Li-rich $Li_{0.5}TiO_2$ (space group *Imma*) phase with orthorhombic symmetry. It has been demonstrated that the Li ions are randomly distributed over half of the available interstitial octahedral sites, which leads to a Li storage capacity of 0.5 (168 mAh g^{-1}).[25] Besides this faradaic process, other types of surface storage mechanisms, connected with pseudo capacities, have been studied. These capacitive effects appear to be strictly connected with the dimensions, the porosity, and the surface area of the material.[26] The cyclic voltammogram of TiO_2-c clearly indicated better kinetics for this material. The intensities of the peaks suggested that the high-surface-area materials exhibit the higher capacities. This has been confirmed by galvanostatic cycling measurements.

Figure 4a shows the first galvanostatic cycle obtained from the three anatase materials at 1 C (0.335 A g^{-1}) between 1.2 and 3 V. The voltage profile of the first discharge of the three investigated materials presents three distinct regions:

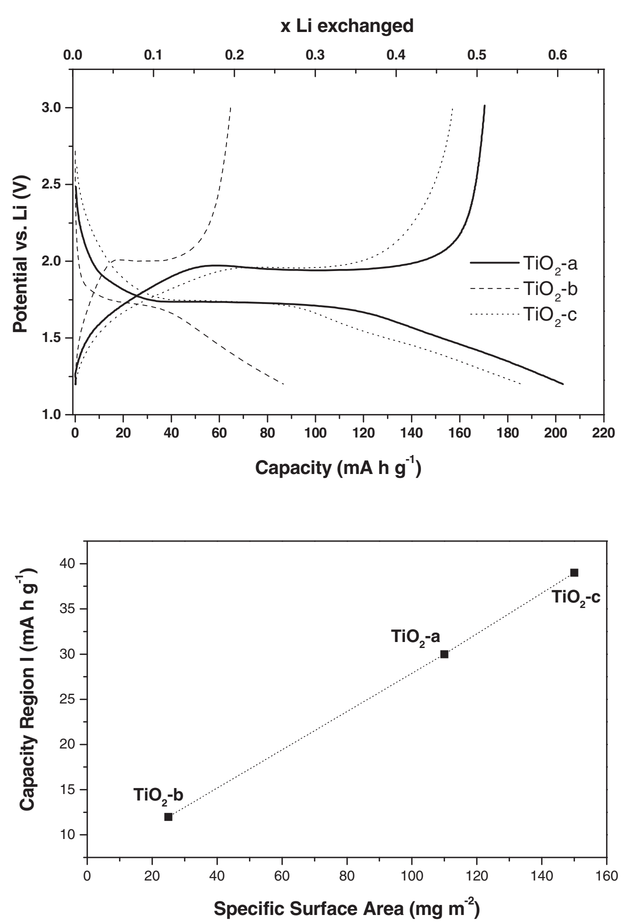

Figure 4. Top: First galvanostatic Li insertion/extraction curves at 1 C of TiO_2-a, TiO_2-b, and TiO_2-c. Bottom: Evolution of the capacity of domain I versus specific surface area.

Table 2. Summary of the capacities measured for the different electrochemical processes during the first cycle for TiO_2-a, TiO_2-b, and TiO_2-c anatase electrodes at 1 C (0.335 A g^{-1}) between 1.2 and 3 V.

Sample	Domain I	Domain II	Domain III	Capacity 1st discharge	Capacity 1st charge	Irreversible capacity
TiO_2-a	30	115	56	201	171	30
TiO_2-b	12	43	31	86	64	22
TiO_2-c	39	92	53	184	154	30

- The first region (I) before a constant-voltage plateau (>1.78 V) is characterized by a potential drop attributed to the formation of the conductive Li_xTiO_2 in the solid-solution domain.[11c] The extent of this domain is directly proportional to the specific surface area of the materials (Figure 4b).
- The second region (II) shows a plateau at 1.78 V, which is attributed to a well-known two-phase mechanism described above.
- The third region (III) at potential below 1.5 V exhibits a sloped curve. This process involves surface lithium storage. The extent of this domain depends on the surface area of the material.

Table 2 summarizes the capacities measured for the different electrochemical processes during the first cycle. From these data, it can be seen that TiO_2-a showed the longest plateau at 1.78 V and a large third region leading to the highest capacity. A very short plateau is observed for TiO_2-b as well as a short third region. Despite its low crystallite size, this material exhibited only poor electrochemical behavior. The high connectivity between primary particles of TiO_2-b prevented the penetration of the electrolyte into the agglomerates of the material. On the contrary, the large surface area of TiO_2-c leads to a very large first region, a short plateau, and a large third region leading to a first discharge capacity of 184 mAh g^{-1}. **Figure 5** presents the comparison of specific charge/discharge capacity of the different electrodes cycled between 1.2 and 3 V upon increasing current values from 1 to 3 C. The best capacity retention is obtained with TiO_2-a. This material presented capacities of 160, 144, and 133 mAh g^{-1} at 1 to 3 C cycling rate. It is interesting to note the increase of capacity observed for TiO_2-b during the first 20 cycles. This rather unusual behavior can be attributed to an enhancement of electrode/electrolyte contact generated upon cycling. Moreover, this material showed an excellent stability in all the investigated charging rates. On the contrary, TiO_2-c presented high initial capacity but less stability. Indeed, after only 20 cycles at the C rate, the capacity retention of TiO_2-c was 90% while it was 95% for TiO_2-a.

The rate capabilities of TiO_2-a and TiO_2-c at charging rates ranging from 1 to 25 C between 1.2 and 3 V are shown in **Figure 6**. Galvanostatic Li insertion/extraction into TiO_2 was carried out for three cycles at charging rates ranging from 1 to 25 C, and the capacities of each material were determined from the third charge curve.

The two materials (TiO_2-a and TiO_2-c) exhibited high rate capabilities. As expected, the reversible capacity decreased with increasing charging rate; however, the capacity decay was less pronounced for TiO_2-c than for TiO_2-a. The best performance was displayed by TiO_2-a (up to 10 C rate). At higher charging rates TiO_2-c showed superior Li rate capabilities (e.g., at 25 C the reversible capacity is 88 mAh g^{-1} for TiO_2-c and 78 mAh g^{-1} for TiO_2-a). The rate capability results of TiO_2-c and TiO_2-a suggest higher surface Li storage abilities for both materials consistent with their high surface area. In the case of TiO_2-b, the low capacities are due to a low surface contact between the electrode material and the electrolyte.

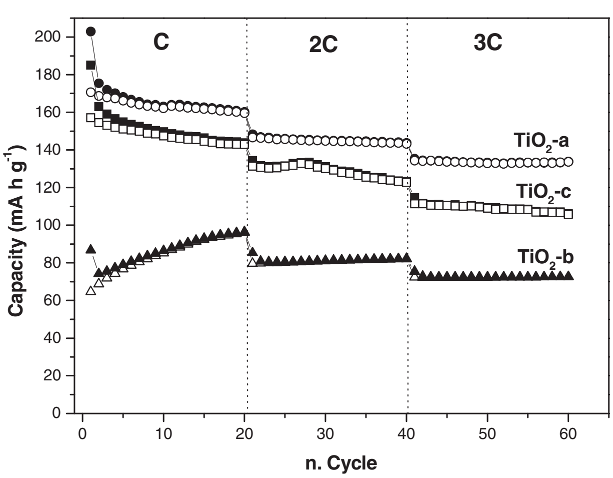

Figure 5. Specific charge/discharge capacity of TiO_2-a, TiO_2-b, and TiO_2-c at different C rate using 1.2–3 V potential windows.

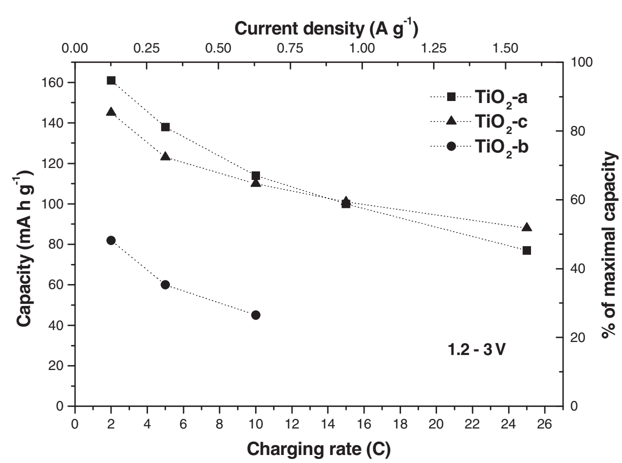

Figure 6. Rate capabilities of TiO_2-a, TiO_2-b, and TiO_2-c using the 1.2–3 V potential range.

small

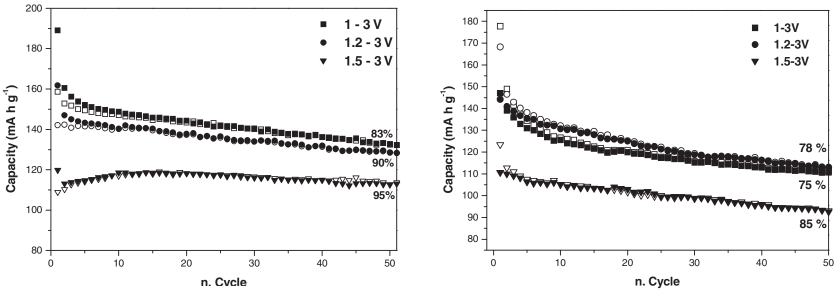

Figure 7. Capacity of lithium insertion/extraction versus charging rate for TiO_2-a (left) and TiO_2-c (right) using 1.5 –3, 1.2 –3, and 1 –3 V potential ranges.

The stability of TiO_2-a and TiO_2-c using different working potential windows has been investigated. For this, repetitive charge/discharge at a relatively high rate (4 C, 1.34 A g^{-1}) was carried out for 50 cycles using three potential ranges (1 –3, 1.2 –3, and 1.5 –3 V). The graphs showing the charge/discharge capacity versus cycle number are presented in **Figure 7**.

The data show that both materials exhibit equivalent initial capacity in all the investigated potential windows. These results are shown in **Table 3** where Q_{rev}, Cap.ret., and ICL represent the reversible capacity, the capacity retention, and the irreversible capacity loss, respectively. After 50 cycles at 4 C, TiO_2-a exhibits 120 (1.5–3 V), 128 (1.2–3 V), and 133 mAh g^{-1} (1.2–3 V) whereas TiO_2-c shows 80, 103, and 97 mAh g^{-1} under the same conditions. Furthermore, TiO_2-a showed a remarkable stability with a capacity retention of 95% after 50 cycles at 4 C. In contrast, a marked capacity fading is observed for TiO_2-c in all investigated potential ranges (capacity retention of 85% after 50 cycles).

From these results, it appears that the stability of the materials depends not only on the morphology but also on the working potential window. In the potential range 1.5–3 V the difference in stability is attributed to the difference in morphology of the two materials; TiO_2-a has a lower surface area and a narrower pore size distribution than TiO_2-c. This arrangement leads to a higher stability in this potential range. Enlarging the potential window to 1–3 V leads to higher Li surface storage and consequently to a higher structure instability upon lithium insertion/extraction, which constitutes a disadvantage for the higher surface area electrode. Therefore the mesoporous TiO_2-a can be considered as a good compromise to obtain both high rate capabilities and high stability.

3. Conclusion

We have demonstrated the effect of optimizing the active material's morphology to obtain enhanced electrochemical performance of anatase TiO_2 anodes. We showed that a mesoporous arrangement is a key morphology to optimize surface kinetics while retaining electrode stability, as demonstrated by the rate capabilities and capacity retention of electrodes with this morphology.

Three different synthetic routes for the preparation of these titania materials were utilized to obtain the different morphological patterns of the samples. Two types of samples were prepared by the sol–gel method in the presence of surfactants (TiO_2-a and TiO_2-b) while TiO_2-c was prepared via a miniemulsion process.

Additionally, the impact of the cycling conditions on the performance of the anatase materials, especially the working potential window, was investigated. It was found that enlarging the cycling potential window led to higher capacities but also to lower stability of the electrode materials.

4. Experimental Section

Materials: All chemicals were employed without further purification: polyethylene-***block***-polyoxyethylene copolymer (PE-***b***-PEO, Brij56, $M_w \approx 682$ g mol^{-1}) was bought from Aldrich; tetraisopropylorthotitanate (TIP, 98%), ethylene glycol (EG, 99.5%), hydrochloric acid, octadecylamine (90%), acetone (99%), and absolute ethanol were purchased from Merck whereas Isopar M was bought from Caldic.

Poly(ethylene/butylene-***block***-ethylene oxide) (P(E/B-***b***-EO); $M_w \approx$ 12 000 g mol^{-1}) was prepared by coupling "Kraton liquid" (M_w = 3900 g mol^{-1}; ω-hydroxypoly(ethylene-***co***-butylene)) with ethylene oxide by anionic polymerization.[27] Demineralized water was used during the experiments.

Precursor: Bis(2-hydroxyethyl)titanate (EGMT) was synthesized by a modified procedure of Xia and co-workers,[20] which was described in detail previously.[21]

Synthesis of TiO_2:

- *TiO_2*-a (Brij56): In a synthesis according to the protocol described in Reference [22], Brij56 (1.23 g, 1.8 mmol) was dissolved by ultrasound in dilute hydrochloric acid (300 mL, pH 2). EGMT (0.29 g, 60 mmol Ti) was added to this solution. The resulting suspension was aged in an oven at 60 °C for 1 day and subsequently annealed at 400 °C for 4 h in air for complete surfactant removal.

Table 3. Summary of cycling data for TiO_2-a and TiO_2-c anatase electrodes in different potential ranges at 4 C (1.34 A g^{-1} charge/discharge rate).

	1–3 V		1.2–3 V		1.5–3 V	
	TiO_2-a	TiO_2-c	TiO_2-a	TiO_2-c	TiO_2-a	TiO_2-c
Q_{rev} (initial) [mAh g^{-1}]	190	177	162	168	120	123
Q_{rev} (50 cycles) [mAh g^{-1}]	133	97	128	103	112	80
Cap. ret. [%]	83	75	90	78	95	85
ICL [mAh g^{-1}]	31	31	20	27	11	14

- *TiO_2-b*: A synthesis modified according to Reference [23] was applied. Octadecylamine (5.35 g, 19.8 mmol) was dissolved by ultrasound in absolute ethanol (60 mL). TIP (8.87 g, 30 mmol) was added to this solution. Demineralized water was sonicated and the ethanolic TIP/octadecylamine solution was added dropwise. Ultrasound was employed for 4 h at 100 W cm $^{-2}$ (22% of the total amplitude). After that the sample was stored in an oven overnight at 60 °C. The sample was then washed several times with water and ethanol and the resulting powder was annealed at 450 °C for 5 h in air.
- *TiO_2-c* (miniemulsion): Titania particles were synthesized in an inverse miniemulsion. The dispersed aqueous phase consisted of EGMT (3.13 g) and hydrochloric acid (100 mL, 1 M). Isopar M (250 g) and P(E/B-*b*-EO) (750 mg, surfactant) were used as continuous organic phase. The system was homogenized by high pressure (continuously for 15 min, starting pressure: 1350 bar, final pressure: 650 bar). After homogenization the miniemulsion was stirred at 100 °C for 18 h. The obtained TiO_2 powders were separated by centrifugation, washed several times with water and acetone, and annealed at 400 °C for 4 h.

Characterization: XRD measurements were performed by using $Cu_{K\alpha}$ radiation (λ = 0.154 nm) on a Siemens D5000 instrument. TEM characterization was carried out on a Cs-corrected FEI Titan microscope operated at 80 kV and on a Phillips CM 20 microscope operating at 200 kV. The samples were dispersed in ethanol and spread on a carbon-coated copper grid. For high-resolution TEM the samples were embedded in resin and cut with an ultramicrotome. The flakes were collected with a copper grid. Nitrogen sorption measurements were performed at 77 K on a Quadrasorb SI instrument (Quantachrome). The surface area was calculated according to the five-point model of Brunauer, Emmett, and Teller (BET) in the p/p_0 range of 0.08–0.26.

Electrode Preparation and Electrochemical Measurements: The electrode materials were prepared by mixing the active material (76 wt.%) with conducting carbon black additive (Super P, 12 wt.%) and poly(vinylidene fluoride) (PVDF) binder (12 wt.%) in *N*-methylpyrrolidone (NMP). The well-mixed slurry was coated onto an aluminum foil using the doctor-blade method. The coated foil was allowed to dry in an oven at 80 °C overnight. It was cut into circular disks and assembled into sealed three-electrode cells under an Ar atmosphere in a glovebox. These disks were used as working electrode, Li metal as counter and reference electrodes, glass fiber (GF/A) from Whatman as separator, and 1 M $LiPF_6$/ethylene carbonate (EC) + dimethyl carbonate (DMC) (1:1, w/w; UBE Industry, Japan) as the electrolyte. Cycling tests were performed at room temperature in the voltage ranges 1.5–3 and 1.2–3 V. The maximum Li insertion into anatase TiO_2 was assumed to be 0.5 (168 mAh g^{-1}), and thus the charging rates were based on the following relationship: 1 C = 0.168 A g^{-1}.

Acknowledgements

Financial support from the DFG under the SPP1181 program is gratefully acknowledged.

[1] a) A. S. Aricó, P. Bruce, B. Scrosati, J. M. Tarascon, W. van Schalkwijk, *Nat. Mater.* **2005**, *4*, 366–377; b) P. G. Bruce, *Solid State Ionics* **2008**, *179*, 752–760; c) P. G. Bruce, *Chem. Commun.* **1997**, *19*, 1817–1824.
[2] a) S. Panero, B. Scrosati, M. Wachtler, F. Croce, *J. Power Sources* **2004**, *129*, 90–95; b) M. Wagemaker, W. J. H. Borghols, F. M. Mulder, *J. Am. Chem. Soc.* **2007**, *129*, 4323–4327; c) P. Poizot, S. Laruelle, S. Grugeon, L. Dupont, J.-M. Tarascon, *Nature* **2000**, *407*, 496–499; d) F. Badway, I. Plitz, S. Grugeon, S. Laruelle, M. Dolle, A. S. Gozdz, J.-M. Tarascon, *Electrochem. Solid-State Lett.* **2002**, *5*, A115–A118.
[3] a) D. Murphy, R. Cava, S. Zahurak, A. Santoro, *Solid State Ionics* **1983**, *9–10*, 413–417; b) B. Zachau-Christiansen, K. West, T. Jacobsen, S. Atlung, *Solid State Ionics* **1988**, *28–30*, 1176–1182; c) D. Dambournet, I. Belharouak, K. Amine, *Chem. Mater.* **2010**, *22*, 1173–1179; d) Z. Yang, D. Choi, S. Kerisit, K. M. Rosso, D. Wang, J. Zhang, G. Graff, J. Liu, *J. Power Sources* **2009**, *192*, 588–598.
[4] a) A.R. Armstrong, G. Armstrong, J. Canales, R. Garcia, P. G. Bruce, *Adv. Mater.* **2005**, *17*, 862–865; b) A. R. Armstrong, G. Armstrong, J. Canales, P. G. Bruce, *J. Power Sources* **2005**, *146*, 501–506; c) A. R. Armstrong, G. Armstrong, J. Canales, P. G. Bruce, *Angew. Chem. Int. Ed.* **2004**, *43*, 2286–2288; d) M. Zukalova, M. Kalbac, L. Kavan, I. Exnar, M. Grätzel, *Chem. Mater.* **2005**, *17*, 1248–1255.
[5] D.-H. Lee, J.-G. Park, Kyoung J. Choi, H.-J. Choi, D. Kim, *Eur. J. Inorg. Chem.* **2008**878–882; b) A. Reddy, M. S. Kishore, V. Pralong, U. V. Varadaraju, B. Raveau, *Electrochem. Solid-State Lett.* **2007**, *10*, A29–A31.
[6] a) T. Ohzuku, Z. Takehara, S. Yoshizawa, *Electrochim. Acta* **1979**, *24*, 219–222; b) L. Kavan, D. Fattakhova, R. Krtil, *J. Electrochem. Soc.* **1999**, *146*, 1375–1379.
[7] a) Y. S. Hu, L. Kienle, Y. G. Guo, J. Maier, *Adv. Mater.* **2006**, *18*, 1421–1426; b) M. A. Reddy, M. S. Kishore, V. Pralong, V. Caignaert, U. V. Varadaraju, B. Raveau, *Electrochem. Commun.* **2006**, *8*, 1299–1303; c) P. Kubiak, M. Pfanzelt, J. Geserick, U. Hörmann, N. Hüsing, U. Kaiser, M. Wohlfahrt-Mehrens, *J. Power Sources* **2009**, *194*, 1099–1104; d) M. Pfanzelt, P. Kubiak, M. Wohlfahrt-Mehrens, *Electrochem. Solid-State Lett.* **2010**, *13*, A91–A94.
[8] a) C. Jiang, M. Wei, Z. Qi, T. Kudo, I. Honma, H. Zhou, *J. Power Sources* **2007**, *166*, 239–243; b) M. Wagemaker, W. J. H. Borghols, F. M. Mulder, *J. Am. Chem. Soc.* **2007**, *129*, 4323–4327; c) G. Sudant, E. Baudrin, D. Larcher, J.-M. Tarascon, *J. Mater. Chem.* **2005**, *15*, 1263–1269; d) L. Kavan, J. Rathousky, M. Grätzel, V. Shklover, A. Zukal, *J. Phys. Chem. B* **2000**, *104*, 12012–12020.
[9] a) T. Ozhuku, T. Kodama, T. Hirai, *J. Power Sources* **1985**, *14*, 153–166; b) S. Huang, L. Kavan, I. Exnar, M. Grätzel, *J. Electrochem. Soc.* **1995**, *142*, L142–L144; c) L. Kavan, M. Grätzel, J. Rathousky, A. Zukal, *J. Electrochem. Soc.* **1996**, *143*, 394–400.
[10] W. J. Macklin, R. J. Neat, *Solid State Ionics* **1992**, *53–56*, 694–700.
[11] a) W. Borghols, D. Lützenkirchen-Hecht, U. Haake, E. van Eck, F. Mulder, M. Wagemaker*Phys. Chem. Chem. Phys.* **2009**, *11*, 5742–5748; b) U. Lafont, D. Carta, G. Mountjoy, A. V. Chadwick, E. M. Kelder, *J. Phys. Chem. C* **2010**, *114*1372–1378.
[12] P. G. Bruce, B. Scrosati, J.-M. Tarascon, *Angew. Chem. Int. Ed.* **2008**, *47*, 2930–2946.
[13] a) L. Kavan, J. Rathousky, M. Grätzel, V. Shklover, A. Zukal, *Microporous Mesoporous Mater.* **2001**, *44–45*, 653–659; b) I. Moriguchi, R. Hidaka, H. Yamada, T. Kudo, *Solid State Ionics* **2005**, *176*, 2361–2366; c) D. Fattakhova, M. Wark, T. Brezesinski, B. Smarsly, J. Rathousky, *Adv. Funct. Mater.* **2007**, *17*, 123–132; d) P. Kubiak, J. Geserick, N. Hüsing, M. Wohlfahrt-Mehrens, *J. Power Sources* **2008**, *175*, 510–516; e) K. Saravanan,

K. Ananthanarayanan, P. Balaya, *Energy Environ. Sci.* **2010**, *3*, 939–948.
[14] B. L. He, B. Dong, H. L. Li, *Electrochem. Commun.* **2007**, *9*, 425–430.
[15] H. S. Zhou, D. L. Li, M. Hibino, I. Honma, *Angew. Chem. Int. Ed.* **2005**, *44*, 797–802.
[16] Y. G. Guo, Y. S. Hu, W. Sigle, J. Maier, *Adv. Mater.* **2007**, *19*, 2087–2091.
[17] a) I. Moriguchi, R. Hidaka, H. Yamada, T. Kudo, H. Murakami, N. Nakashima, *Adv. Mater.* **2006**, *18*, 69–73; b) D. Wang, D. Choi, J. Li, Z. Yang, Z. Nie, R. Kou, D. Hu, C. Wang, L. V. Saraf, J. Zhang, I. A. Aksay, J. Liu, *ACS Nano* **2009**, *3*, 907–914; c) Y. Ishii, Y. Kanamori, T. Kawashita, I. Mukhopadhyay, S. Kawasaki, *J. Phys. Chem. Solids* **2010**, *71*, 511–514.
[18] B. Erjavec, R. Dominko, P. Umek, S. Sturm, S. Pejovnik, M. Gaberscek, J. Jamnik, *Electrochem. Commun.* **2008**, *10*, 926–929.
[19] a) M. Mancini, P. Kubiak, M. Marassi, M. Wohlfahrt-Mehrens, *J. Power Sources* **2009**, *189*, 585–589; b) M. Mancini, P. Kubiak, M. Marassi, M. Wohlfahrt-Mehrens, *J. Electrochem. Soc.* **2010**, *157*, A164–A170.
[20] X. Jiang, T. Herricks, Y. Xia, *Adv. Mater.* **2003**, *15*, 1205–1209.
[21] J. Geserick, N. Hüsing, R. Rosmanith, K. Landfester, C. K. Weiss, Y. Denkwitz, R. J. Behm, U. Hörmann, U. Kaiser, *Mater. Res. Soc. Symp. Proc. 1007*, Materials Research Society, Boston, **2008**, pp.S04–S13.
[22] Y. Q. Wang, S. G. Chen, X. H. Tang, O. Palchik, A. Zaban, Y. Koltypin, A. Gedanken, *J. Mater. Chem.* **2001**, *11*, 521–526.
[23] a) R. Rossmanith, C. K. Weiss, J. Geserick, N. Hüsing, U. Hormann, U. Kaiser, K. Landfester, *Chem. Mater.* **2008**, *20*, 5768–5780; b) R. Schiller, C. K. Weiss, J. Geserick, N. Husing, K. Landfester, *Chem. Mater.* **2009**, *21*, 5088–5098; c) R. Schiller, C. K. Weiss, K. Landfester, *Nanotechnology* **2010**, *21*, 405603.
[24] R. Van de Krol, A. Goossens, E. Meulenkamp, *J. Electrochem. Soc.* **1999**, *146*, 3150–3154.
[25] a) A. Stashans, S. Lunell, R. Bergström, A. Hagfeldt, S.-E. Lindquist, *Phys. Rev. B* **1996**, *53*, 159–170; b) L. Kavan, M. Grätzel Rathouskỳ, A. Zukal, *J. Electrochem. Soc.* **1996**, *143*, 394–400; c) H. Lindstrom, S. Södergren, A. Solbrand, H. Rensmo, J. Hjelm, A. Hagfeldt, S.-E. Lindquist, *J. Phys. Chem. B* **1997**, *101*, 7717–7722; d) M. Wagemaker, A. Kentgens, F. Mulder, *Nature* **2002**, *418*, 397–399; e) R. Baddour-Hadjean, S. Bach, M. Smirnov, J.-P. Pereira-Ramos, *J. Raman Spectrosc.* **2004**, *35*, 577–585.
[26] J. Wang, J. Polleux, J. Lim, B. Dunn, *J. Phys. Chem. C* **2007**, *111*, 14925–14931.
[27] A. Thomas, H. Schlaad, B. Smarsly, M. Antonietti, *Langmuir* **2003**, *19*, 4455–4459.

Received: October 31, 2010
Revised: January 24, 2011
Published online:

